Available online at www.sciencedirect.com
ScienceDirect
Journal of the European Ceramic Society 27 (2007) 4333–4337
www.elsevier.com/locate/jeurceramsoc

Chemical vapor synthesis and characterization of chromium doped zinc oxide nanoparticles

Wei Jin, In-Kyum Lee, Alexander Kompch, Udo Dörfler, Markus Winterer*

Nanoparticle Process Technology, Department of Engineering Science and Center for Nanointegration Duisburg-Essen (CeNIDE), University Duisburg-Essen, Lotharstr. 1, D-47057 Duisburg, Germany

Available online 9 April 2007

Abstract

ZnO and Cr doped ZnO nanoparticles were synthesized by chemical vapor synthesis (CVS) which is a modified chemical vapor deposition (CVD) process. The resulting powders consist of nanocrystalline particles and were characterized by X-ray diffraction (XRD), nitrogen adsorption (BET), transmission electron microscopy (TEM), energy dispersive X-ray analysis (EDX), element analysis, and extended X-ray absorption fine structure (EXAFS) spectroscopy. The grain size decreases with increasing dopant concentration. The lattice constants extracted by the Rietveld method from XRD data vary slightly with doping concentration. XRD and EXAFS data analysis show that the Chromium dopant atoms are incorporated into the wurtzite host lattice.

Keywords: Powders-gas phase reaction; X-ray methods; Spectroscopy; ZnO; Chemical vapor synthesis (CVS)

1. Introduction

Zinc oxide is a II–VI semiconductor with a wide direct band gap of 3.37 eV and a large exciton binding energy of 60 meV at room temperature which makes it suitable as material for blue and ultraviolet light-emitting devices.[1] In the past years ZnO has received more and more attentions due to their potential applications, such as short-wavelength optoelectronics[2] and transparent conductive films for solar cells.

A number of synthetic routes have been employed to synthesize ZnO nanoparticles, such as sol–gel chemistry,[3–7] spray pyrolysis,[8] metal-organic chemical vapor deposition,[9,10] flame synthesis,[11] cathodic electrodeposition,[12,13] plasma pyrolysis[9] and chemical vapor synthesis.[14] Ball milling and spray pyrolysis has been used to prepare nanostructured Zn–Cr–O spinel powders.[15,16]

The properties of ZnO nanoparticles can be adjusted by their size and by introducing dopants. Ab initio calculations predict ferromagnetism in ZnO doped with most transition metal ions, such as Fe, Ni, Co, and Cr.[17] The band gap of ZnO can be tuned by doping.[18] Recently, Roberts et al. synthesized Cr doped ZnO via magnetron sputtering. They found ferromagnetic ordering with a room temperature saturation moment of 1.4 μ_B per Cr ion at a doping concentration of 9.5 at.% after annealing in UHV.[19] Potential applications of ferromagnetic semiconductors include electrically controlled magnetic sensors and actuators, high density ultralow-power memory and logic, spin-polarized light emitters for optical encoding, advanced optical switches and modulators and devices with integrated magnetic, electronic and optical functionality.[20]

However, the origin of the magnetic properties and especially the structure of the magnetic dopants is presently under discussion.[21] Therefore, in this paper we report on the Chemical vapor synthesis (CVS) of nanocrystalline Cr doped ZnO and the structural characterization of the corresponding products with emphasis on the local structure around Cr atoms. Magnetooptic investigations will be publised elsewhere.

2. Experimental details and data analysis

Fig. 1 shows the experimental setup of the CVS reactor. It consists of two sequential hot zones for evaporating and pyrolysis of the solid precursors, respectively. The hot zones consist of an alumina tube placed into the two sequential furnaces. The precursors are evaporated from alumina boats in the first hot zone and then transported by helium carrier gas into the second hot zone. Zinc acetylacetonate ($Zn(acac)_2$) and Chromium

* Corresponding author.
E-mail address: markus.winterer@uni-due.de (M. Winterer).

0955-2219/$ – see front matter © 2007 Elsevier Ltd. All rights reserved.
doi:10.1016/j.jeurceramsoc.2007.02.152

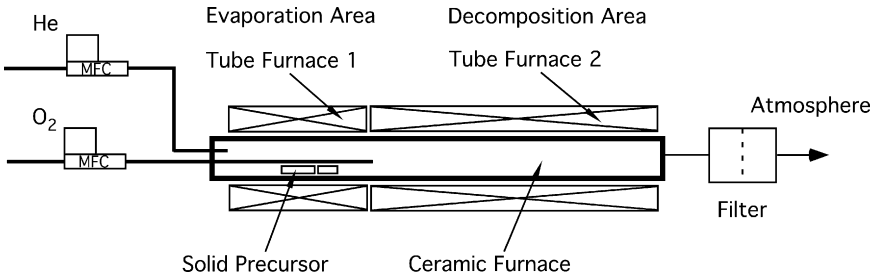

Fig. 1. Experimental setup of the CVS reactor for production of doped nanocrystalline ZnO powders.

acetylacetonate ($Cr(acac)_3$) were used as precursors for the chemical vapor synthesis of Chromium doped Zinc oxide. In the second hot zone the precursors are pyrolysed and oxidized by additional oxygen at 1173 K. The process pressure is ambient. The particles are then collected on a paper filter at the reactor exit. The evaporation rate of the precursors was investigated by means of thermogravimetric analysis (TGA) in order to control the dopant concentration and particle size. The alumina boats for Cr- and Zn-precursors were placed at different positions in the first furnace thereby exploiting the temperature profile to vary the evaporation rate according to the TGA results. For pure ZnO the maximum temperature in the first furnace was 493 K and for the doped samples 423 K. The composition (dopant content, also used to designate the sample in this paper) of the samples was determined by energy dispersive X-ray analysis with an EDX system ISIS 300 with an EDX 7370 detector.

Crystal structure and phase composition of the samples were determined by X-ray diffraction using a PANalytical X-ray diffractometer (X'Pert PRO) with Cu Kα (1.54184 Å) and Co Kα (1.54184 Å) radiation and an X'Celerator detector. The XRD data were collected in a range of $25^\circ < 2\theta < 100^\circ$ with a step size of 0.05°. The diffraction data were analyzed by means of Rietveld refinement using the program FULLPROF.[22] The XRD diffractograms were analyzed using the wurtzite structure (space group $P6_3mc$, No. 186) with initial structural parameters taken from the ICSD data base (collection code 65119). Information on the isotropic microstrain and grain size broadening are obtained using a Thompson-Cox-Hastings-pseudo-Voigt line shape function.

The TEM specimens were prepared by dispersing the powder in cyclohexane with the aid of ultrasonic agitation. A few drops were poured onto a porous carbon film supported on a copper grid, then dried in air. The TEM image were obtained using a Philips CM 12 electron microscope at an acceleration voltage of 120 kV.

EXAFS spectra were measured at the Zn and Cr K-edge at the XAS beamline at ANKA, Karlsruhe. The sample thickness was optimized for transmission by diluting the appropriate amount of sample homogeneously in cellulose powder and uniaxial pressing of a pellet. Transmission and fluoroescence spectra were collected at room temperature and 15 K. The program xafs[23] was used for EXAFS data reduction. The EXAFS data were analyzed by the Reverse Monte Carlo Method (RMC) using the rmcxas program.[24] Initial atom configurations were generated from results of the Rietveld refinements of X-ray diffraction data of the corresponding samples and contain an appropriate number of chromium atoms. Zn- and Cr-EXAFS spectra were analyzed simultaneously. The theoretical amplitude and phase functions for the RMC analysis were obtained by FEFF8 simulations.[25]

3. Results and discussion

The TEM images in Fig. 2 indicates that the particles have mostly an equiaxial morphology and are agglomerated. Particle size distributions were determined from TEM images. Fig. 2(a) displays pure ZnO nanoparticles with a mean diameter of 27 nm and Fig. 2(b) shows a Cr doped ZnO sample containing a 6 at.% Cr with a mean diameter of 18 nm. The dopant concentrations of Cr in ZnO matrix were determined by energy dispersive X-ray analysis. Element analysis by combustion revealed that the concentration of the carbon and hydrogen in the samples are less than 0.5 wt% which indicates that the precursors were completely decomposed under conditions of synthesis.

Fig. 3 shows the XRD pattern of a 3 at.% Cr doped ZnO sample analyzed with Rietveld refinement. The refined pattern is in very good agreement with the measured data. No second phase is observed which is a first indication that the dopant atoms are incorporated in the wurtzite structure. Fig. 4 shows that the lattice parameter of the *a*-axis decreases and the lattice parameter of the *c*-axis increases with increasing dopant concentration. This observation is another indication that the dopant atoms have been incorporated into the wurtzite crystal structure. The lattice parameter of the pure oxide differs from the literature bulk value (Fig. 4)[26] probably because the point defect concentration (oxygen vacancies and zinc interstitials)[27] are larger for the CVS powders compared to the single crystals prepared hydrothermally.

The crystallite size decreases with increasing dopant concentration (19 nm for pure ZnO and 8 nm at 6 at.%). One important elementary step in CVS is the sintering of primary particles within agglomerate. The kinetics of this process are influenced by the dopant atoms as the mobility of the grain boundaries in the agglomerate is limited by impurity drag.[27] Other possible grain growth inhibition mechanisms such as segregation, second phase precipitation or processes influencing the nucleation can not be ruled out. However, nucleation phenomena seem unlikely as the CVS process is based on irreversible decomposition reactions of the precursor, second phases have not been observed with the detection limits of XRD and EELS showed a homogeneous distribution of chromium across the particles investigated.

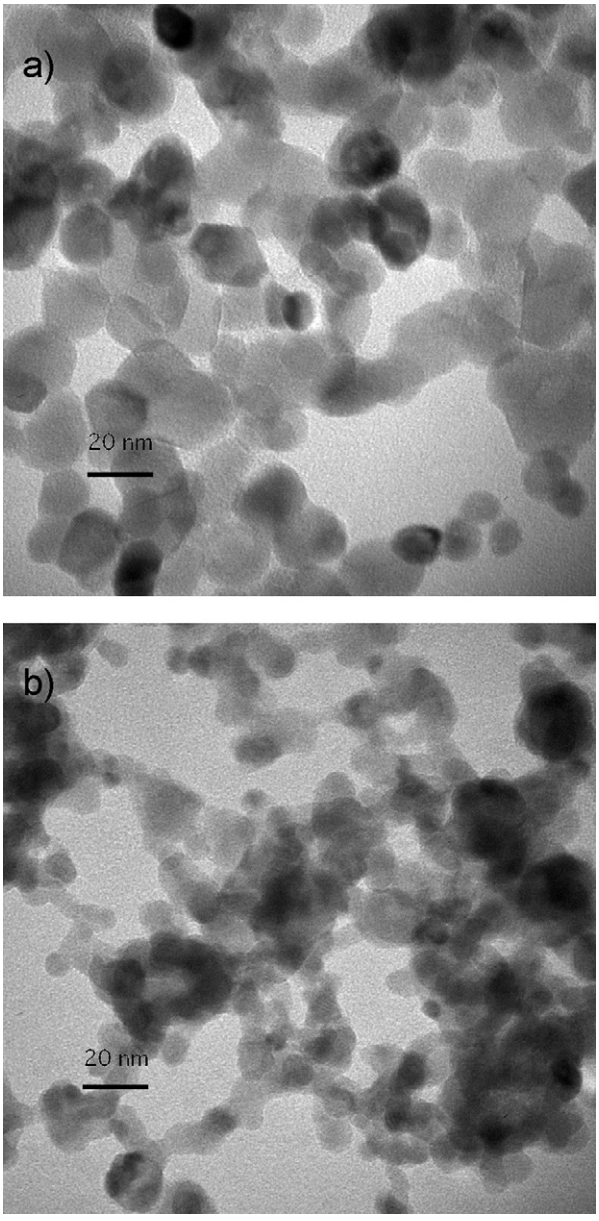

Fig. 2. TEM images of CVS nanoparticles (a) pure ZnO, (b) 6 at.% Cr doped ZnO.

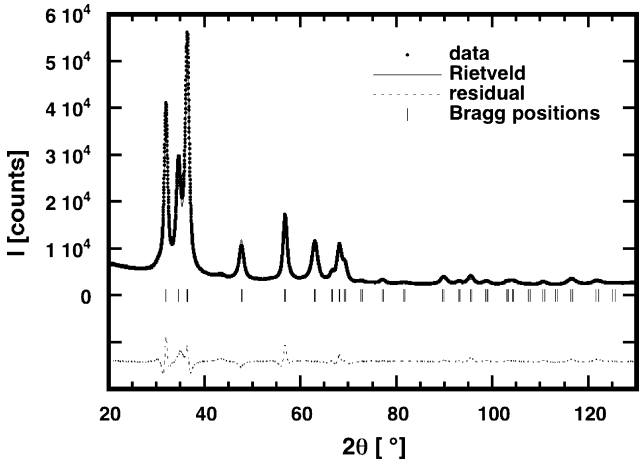

Fig. 3. X-ray diffractogram with Rietveld refinement of a 3 at.% Cr doped ZnO.

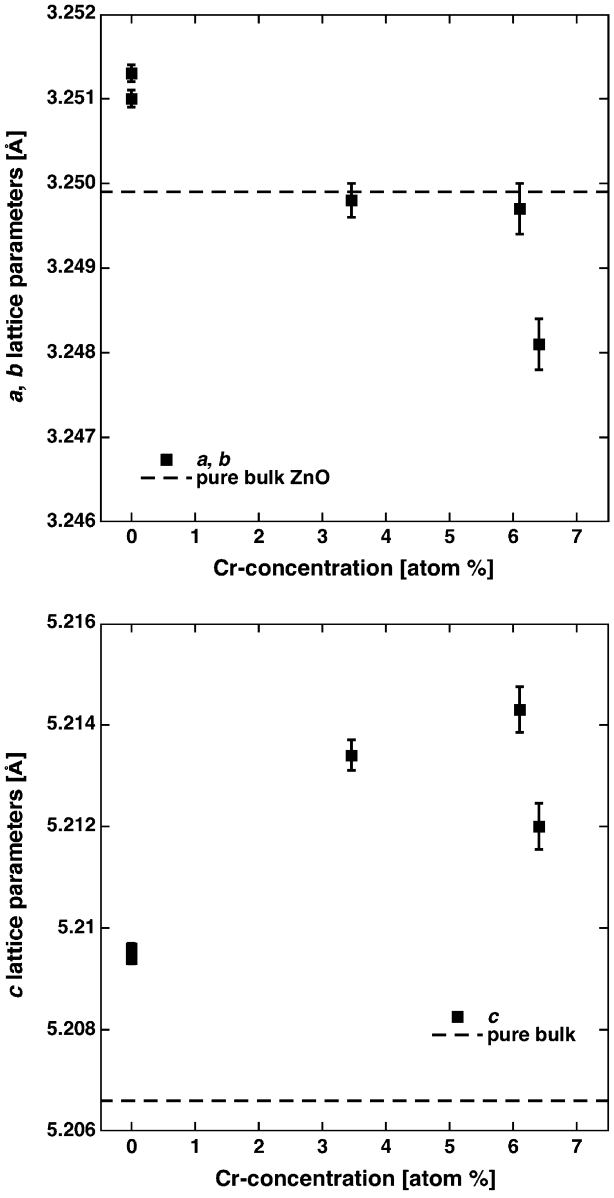

Fig. 4. Lattice constants *a*, *b* (top) and *c* (bottom) as a function of dopant concentration, and comparison with bulk values for pure ZnO from the literature[26].

EXAFS spectroscopy as a probe for the local structure around X-ray absorbing atoms provides more information about the location of the dopant atoms in the wurtzite structure. According to the RMC analysis of a sample containing 3 at.% chromium, the oxygen coordination number of Cr is four which is consistent with a tetrahedral coordination excluding the octahedral interstitial site. However the corresponding peak in the Cr–O partial pair distribution function (Fig. 5, left) is split which can be explained by a distortion of the coordination polyhedron. This agrees with the observation that the Zn–Cr and Cr–Cr partial pair distribution function do not completely overlap with the Zn–Zn partial pair distribution function which would be the case if all Cr atoms are located on substitutional Zn sites. A comparison of the cationic partial distribution functions (Fig. 5, right), reveals that only part of the Cr–Cr and Zn–Zn distances agree with the Zn–Zn distribution function. These can be attributed to Cr atoms

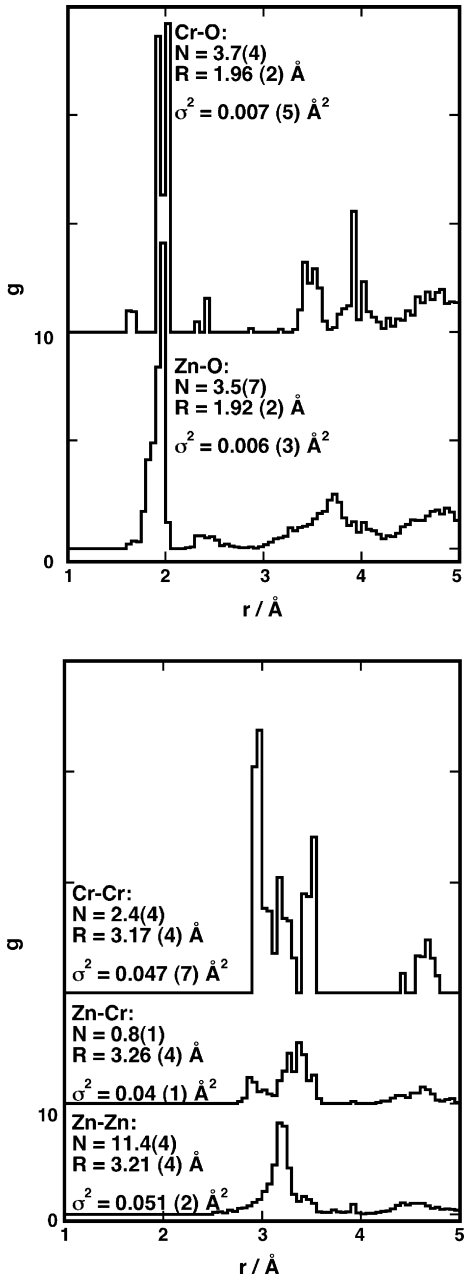

Fig. 5. Partial pair distribution functions (cation-oxygen: left; cationic: right) from EXAFS data using RMC analysis of a 3 at.% Cr doped ZnO sample and results of moment analysis of the first peaks in the distribution functions.

on substitutional Zn-sites whereas the deviating bond distances can either be explained be phase separation, or by Cr on distorted tetrahedral sites located in the lattice forming the particle or segregated at the particle surface. As discussed before, phase separation seems unlikely as it is neither observed in TEM/EELS nor in XRD.

4. Conclusions

Highly crystalline ZnO and Cr doped ZnO nanoparticles can be produced by the CVS process. The chromium atoms are incorporated into the wurtzite lattice and do not form a second phase. The chromium atoms probably reside partially on ideal and on distorted tetrahedral sites which could be either the substitutional Zn sites or the tetrahedral interstitial sites or a mixture of both. The formation of distorted sites may also be due to a segregation of chromium atoms to the particle surface.

Acknowledgements

The financial support by the German Research Foundation (DFG) through the collaborative research center SFB 445 is gratefully acknowledged. We thank M. Vennemann and H. Zähres (Prof. Farle) for help with XRD and TEM measurements, A. Görnt (Prof. Atakan) for the thermal analysis, P. Hinkel (Prof. Nowak) for EDX measurments and V. Hiltenkamp for elemental analysis. We also gratefully acknowledge the support by ANKA, the synchrotron facility at the Karlsruhe Research Center and the XAS beamline scientist S. Mangold.

References

1. Look, D. C., Recent advances in ZnO materials and devices. *Mater. Sci. Eng. B*, 2001, **80**, 383–387.
2. Wang, X. D., Summers, C. J. and Wang, Z. L., Large-scale hexagonal-patterned growth of aligned ZnO nanorods for nano-optoelectronics and nanosensor arrays. *Nano Lett.*, 2004, **4**, 423–426.
3. Hoyer, P. and Weller, H., Size-dependent redox potentials of quantized zinc-oxide measured with an optically transparent thin-layer electrode. *Chem. Phys. Lett.*, 1994, **221**, 379–384.
4. Bahnemann, D. W., Kormann, C. and Hoffmann, M. R., Preparation and characterization of quantum size zinc oxide: a detailed spectroscopic study. *J. Phys. Chem.*, 1987, **91**, 3789–3798.
5. Haase, M., Weller, H. and Henglein, A., Photochemistry and radiation chemistry of colloidal semiconductors. 23. Electron storage on zinc oxide particles and size quantization. *J. Phys. Chem.*, 1988, **92**, 482–487.
6. Sakohara, S., Tickanen, L. D. and Anderson, M. A., Luminescence properties of thin zinc oxide membranes prepared by the sol–gel technique: change in visible luminescence during firing. *J. Phys. Chem.*, 1992, **96**, 11086–11091.
7. Spanhel, L. and Anderson, M. A., Semiconductor clusters in the sol–gel process: quantized aggregation, gelation, and crystal growth in concentrated ZnO colloids. *J. Am. Chem. Soc.*, 1991, **113**, 2826–2833.
8. De Merchant, J. and Cocivera, M., Preparation and doping of zinc oxide using spray pyrolysis. *Chem. Mater.*, 1995, **7**, 1742–1749.
9. Roth, A. P. and Williams, D. F., Properties of zinc oxide films prepared by the oxidation of diethyl zinc. *J. Appl. Phys.*, 1981, **52**, 6685–6692.
10. Maruyama, T. and Shionoya, J., Zinc oxide thin films prepared by chemical vapour deposition from zinc acetate. *J. Mater. Sci. Lett.*, 1992, **11**, 170–172.
11. Kleinwechter, H., Janzen, C., Knipping, J., Wiggers, H. and Roth, P., Formation and properties of ZnO nano-particles from gas phase synthesis processes. *J. Mater. Sci.*, 2002, **37**, 4349–4360.
12. Izaki, M. and Omi, T., Transparent zinc oxide films prepared by electrochemical reaction. *Appl. Phys. Lett.*, 1996, **68**, 2439–2440.
13. Peulon, S. and Lincot, D., Cathodic electrodeposition from aqueous solution of dense or open-structured zinc oxide films. *Adv. Mater.*, 1996, **8**, 166–170.
14. Brehm, J., Winterer, M. and Hahn, H., Synthesis and local structure of doped nanocrystalline zinc oxides. *J. Appl. Phys.*, 2006, **100**, 064311.
15. Marinkovic, Z. V., Mancic, L. M. and Milosevic, O., Preparation of nanostructured Zn–Cr–O spinel powders by ultrasonic spray pyrolysis. *J. Eur. Ceram. Soc.*, 2001, **21**, 2051–2055.
16. Marinkovic, Z. V., Mancic, L., Vulic, P. and Milosevic, O., Microstructural characterization of mechanically activated ZnO–Cr_2O_3 system. *J. Eur. Ceram. Soc.*, 2005, **25**, 2081–2084.

17. Sato, K. and Katayama-Yoshida, H., Material design for transparent ferromagnets with ZnO-based magnetic semiconductors. *Jpn J. Appl. Phys.*, 2000, **39**, L555–L558.
18. Pearton, S. J., Norton, D. P., Ip, K., Heo, Y. W. and Steiner, T., Recent advances in processing of ZnO. *J. Vac. Sci. Technol. B*, 2004, **22**, 932–948.
19. Roberts, B. K. and Pakhomov, A. B., *J. Appl. Phys.*, 2005, **97**, 10D310.
20. Pearton, S. J., Abernathy, C. R., Overberg, M. E., Thaler, G. T., Norton, D. P., Theodoropoulou, N. *et al.*, Wide band gap ferromagnetic semiconductors and oxides. *J. Appl. Phys.*, 2003, **93**, 1–13.
21. Mandal, S. K., Das, A. K., Nath, T. K. and Karmakar, D., Temperature dependence of solubility limit of transition metals (Co, Mn, Fe, and Ni) in ZnO nanoparticles. *Appl. Phys. Lett.*, 2006, **89**, 144105-1-3.
22. Rodriguez-Carvajal J. LLB, private communication.
23. Winterer, M., XAFS—a data analysis program for materials science. *J. Phys. IV France*, 1997, **7**, C2-243-244.
24. Winterer, M., Reverse Monte Carlo analysis of EXAFS spectra of amorphous and monoclinic zirconia. *J. Appl. Phys.*, 2000, **88**, 5635.
25. Ankudinov, A. L., Ravel, B., Rehr, J. J., Albers, R. C. and Conradson, S. D., Real-space multiple-scattering calculation and interpretation of X-ray-absorption near-edge structure. *Phys. Rev. B*, 1998, **58**, 7565–7576.
26. Albertsson, J., Abrahams, C. and Kvivk, A., Atomic displacement, anharmonic thermal vibration, expansivity and pyroelectric coefficient therman dependencies in ZnO. *Acta Crystallogr. B*, 1989, **45**, 34–40.
27. Chiang, Y. M., Birnie, D. and Kingery, W. D., *Physical Ceramics—Principles for Ceramic Science and Engineering*. Wiley, 1997.